Enhancing Urban Climate-Energy Modeling in the Community Earth System Model (CESM) through Explicit Representation of Urban Air-conditioning Adoption

Authors:

Xinchang 'Cathy' Li[1], Lei Zhao[1,2,3,*], Keith Oleson[4], Yuyu Zhou[5], Yue Qin[6], Keer Zhang[7], Bowen Fang[1]

Affiliations:

[1] Department of Civil and Environmental Engineering, University of Illinois at Urbana-Champaign, Urbana, Illinois, USA.

[2] Institute for Sustainability, Energy, and Environment (iSEE), University of Illinois at Urbana-Champaign, Urbana, Illinois, USA.

[3] National Center for Supercomputing Applications, University of Illinois at Urbana-Champaign, Urbana, Illinois, USA.

[4] National Center for Atmospheric Research, Boulder, Colorado, USA.

[5] Department of Geography and Urban Systems Institute, The University of Hong Kong, Hong Kong, China.

[6] College of Environmental Science and Engineering, Peking University, Beijing, China.

[7] School of the Environment, Yale University, New Haven, Connecticut, USA

* Correspondence to: Lei Zhao (leizhao@illinois.edu)

Abstract

Improved representation of urban processes in Earth System Models (ESMs) is a pressing need for climate modeling and climate-driven urban energy studies. Despite recent improvements to its fully coupled building energy model, the current Community Land Model Urban (CLMU) in the Community Earth System Model (CESM) lacks the infrastructure to model air-conditioning (AC) adoption explicitly. This undermines CESM's fidelity in modeling urban climate and energy use, and limits its use in climate and energy risk assessments. Here, we establish an explicit-AC-adoption parameterization scheme in CESM that represents AC adoption explicitly through an AC adoption rate parameter in the Building Energy Model of CLMU, and build a present-day, global, survey-based, and spatially explicit AC adoption rate dataset at country and sub-country level that is integrated within CESM. The new dataset can be leveraged for other ESMs or global-scale models and analyses. The explicit AC adoption scheme and the AC adoption rate dataset significantly improve the accuracy of anthropogenic heat modeling due to AC in CESM. The new parameterization scheme makes it possible to evaluate the effects of changing AC adoption on global urban energy and climate using CESM. These developments enhance CESM in its use for climate impact assessments under future climate and socioeconomic development scenarios, and represent continued efforts in better representing urban processes and coupled human-urban-Earth dynamics in ESMs.

Key points

1. An explicit air-conditioning adoption scheme is developed for the building energy model in the Community Land Model Urban
2. A global air-conditioning adoption rate dataset is built for CESM, with potential for use in other global-scale models and analyses
3. The new scheme and dataset greatly improve model performance and enable more comprehensive climate and energy risk assessments

Plain Language Summary

Human activities in cities, such as building energy use, need to be better represented in models designed to simulate urban climate around the world. The Community Land Model Urban is one such model that has been continuously improved, but still cannot effectively model varying air conditioning (AC) adoption rate across countries. This limitation hinders the model's ability in simulating urban climate and building energy use. Here, we improve the model by developing a new explicit-AC-adoption parameterization that represents the proportions of buildings with AC systems, and constructing a global AC adoption rate dataset at present-day for all countries and regions in the world. These improvements help the model simulate the air-conditioning energy use more accurately, and provide opportunities to evaluate the combined effects of climate change, population growth, and economic development on building energy use and climates for cities around the world.

MAIN

1. Introduction

There is a growing interest in connecting energy and climate modeling to address the global challenges of climate change and energy security (Craig et al., 2022). Climate change is poised to significantly affect climate-exposed energy supply and demand, and poses significant challenges to climate-sensitive energy system planning and design (van Ruijven et al., 2019; Schaeffer et al., 2012; Taseska et al., 2012; Yalew et al., 2020). Changes to energy supply and usage, in return, affect the biophysical and biogeochemical processes in the climate systems, and require sufficient characterization in models so as to reduce the uncertainties in future climate projections (Allen et al., 2011; Hadley et al., 2006). Earth System Models (ESMs) were initially developed for studying broader-scale dynamics and interactions of the climate systems (Hurrell et al., 2013), and thus their incorporation of human activities, such as urban and building energy representation, are either missing or very rudimentary. It has been shown that anthropogenic heat flux can reach tens or hundreds of W/m^2 in some urban centers (Ichinose et al., 1999; Kikegawa et al., 2014; Wang et al., 2018), making dynamic modeling of urban heating and air conditioning (HAC) energy use vital in closing the urban surface energy balance. Ignoring the anthropogenic heat representation will thus undermine ESMs' fidelity in accurately modeling urban climate. At the same time, ESMs have been increasingly used for purposes beyond large-scale climate dynamics, such as characterizing impacts of energy production/use on climate (Fitch, 2015; Hu et al., 2016; Wang et al., 2019), projecting future energy demand (Deroubaix et al., 2021), or informing policy making on large-scale energy risks and

climate adaptions (IPCC, 2022; Reidmiller et al., 2018), where more detailed and accurate energy and urban parameterizations are necessary. Therefore, improved representations of coupled human-urban-Earth dynamics in ESMs that capture the physics behind the energy-climate feedbacks is a pressing need for both climate modeling and climate-driven urban energy studies (Creutzig et al., 2015; Güneralp et al., 2017; Sharma et al., 2021).

The Community Terrestrial Systems Model (CTSM) is a state-of-the-art global land model that is part of the Community Earth System Model (CESM). It has an urban module, Community Land Model Urban (CLMU) that simulates the states and fluxes over urban landscapes and communicates with other CTSM and CESM components. The CLMU is fully coupled with a simplified Building Energy Model (BEM), where heating and air-conditioning (HAC) energy demand in urban areas are modeled. The HAC energy demand is calculated at each time step as the energy needed to increase (for heating) or decrease (for air conditioning, AC) the interior building temperature to a setpoint temperature. The waste heat generated from the use of HAC is released into the urban canyon at each time step, thus completing the feedback between urban energy use and urban microclimate. The CLMU has been widely evaluated with in-situ and satellite observations across the world (Demuzere et al., 2008, 2014, 2017; Demuzere et al., 2013; Fitria et al., 2019; Karsisto et al., 2016; Lin et al., 2016; Mohammad Harmay & Choi, 2022; Oleson et al., 2008; Oleson & Feddema, 2020; Zhao et al., 2014, 2021) and continuously improved by the community (Fang et al., 2023).

Despite the improvements in urban energy use modeling in CTSM, there is a critical yet longstanding limitation in the current BEM in CLMU: lack of the infrastructure to model AC adoption explicitly. As a global climate model, CESM represents air conditioning in an average setting for each urban density class in a grid cell, instead of modeling individual buildings and their AC systems if any. Currently, AC adoption is implicitly controlled by proxy interior building setpoints, without an explicit AC adoption rate parameter. This parameterization scheme, although viable, undermines the physical interpretability of the model. For example, to signal low AC adoption, the building interior setpoint temperature for AC can be as high as 42°C in some regions (Oleson & Feddema, 2020), which is much higher than what we experience in reality, and only offer qualitative insights to the AC adoption rate of the region. This also means that although the average AC energy flux over an extended period may be accurate, daily or hourly values, which are necessary for the study of extremes, would be largely different from what we may observe in reality. This poses challenges to assuring model accuracy, as the building interior setpoint temperature and AC adoption rate cannot be tuned separately. One can only rely on heuristics specific to a certain location, instead of statistics or documentation on thermostat setpoint or AC adoption rate, if one wishes to fine tune the energy and climate models. This also means that it is not possible to make future projections incorporating changes in AC adoption under various socioeconomic development pathways and climate change scenarios using the current scheme. This further hinders inter-model and inter-regional comparison for climate risk assessments and energy planning.

Climatic and socioeconomic drivers both affect the biophysical feedbacks between urban climate and urban energy use (Figure 1). Warmer background climates will increase urban temperatures, and population and economic growth will fuel urban expansion and higher AC adoption especially in the global south, both of which are positive drivers to the feedback cycle (Kikegawa et al., 2022; Salamanca et al., 2014). AC adoption rate (also called penetration rate or ownership rate) is one of the most widely used parameters in the socioeconomic literature that characterize the changes in AC ownership, defined as the share of households that own at least one AC equipment (system or unit). It is a strong function of temperature and income (Davis & Gertler, 2015), and an essential parameter in econometric or integrated assessment models for making future AC energy use projections (Colelli & Cian, 2020; L. Davis et al., 2021; Mastrucci et al., 2021). Studies have found that globally, socioeconomic factors tend to be stronger drivers of energy demand than climate change in the 21st century (Isaac & van Vuuren, 2009; Rastogi et al., 2019; van Ruijven et al., 2019), which means it will become increasingly more important to integrate socioeconomic factors into future urban climate and energy projections in physics-based dynamic models.

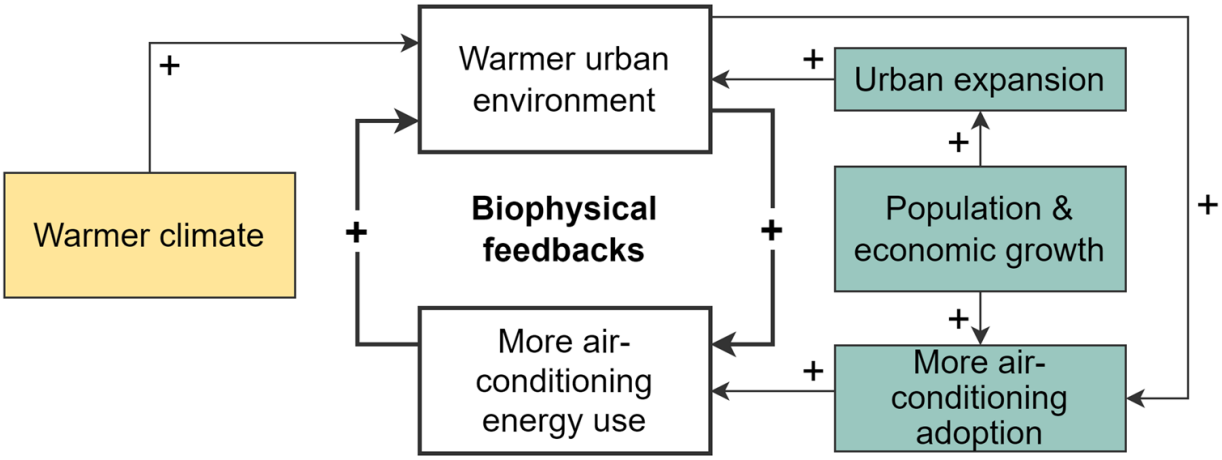

Figure 1. Climatic (in yellow, on the left) and socioeconomic drivers (in teal, on the right) to the biophysical feedbacks between urban climate and urban air-conditioning energy use (in the center, bolded arrows and boxes). The plus signs indicate positive effects.

In this work, we present a new explicit-AC-adoption parameterization scheme in CESM that explicitly represents AC adoption by introducing an AC adoption rate parameter in the BEM of CLMU. In support of this, we build a first-of-its-kind global, survey-based, and spatially explicit AC adoption rate dataset at country and sub-country level integrated in CTSM, and can be leveraged for other global-scale models and analyses in the climate, energy, and socioeconomic fields. The explicit AC adoption scheme and the AC adoption rate dataset together significantly improve the AC energy modeling performance of CTSM. The new parameterization scheme makes it possible to model changes in AC adoption rate and their local to global impacts on urban climate and energy in CESM, where the dynamic interactions between urban climate and energy are modeled.

This paper is organized as follows. Section 2 provides an overview of the CLMU, BEM, and the current AC scheme. The mathematical model for explicit AC adoption is presented in Section 3. Section 4 describes the new global AC adoption rate dataset generated by this work. In Section 5, we describe the simulations we designed to evaluate and test the explicit-AC-adoption parameterization scheme and demonstrate new capabilities, as well as datasets used for validation. Results and discussions follow in Section 6.

2. Overview of CLMU, its Building Energy Model (BEM) and air-conditioning flux modeling

The improvements described in this paper are based on the most recent version of CLMU, first described in Oleson & Feddema (2020), referred to hereinafter as CLMU5. An overview of CLMU5, its Building Energy Model (BEM) and its air-conditioning flux parameterization is provided below for the context of discussion.

Grid cells in CTSM can have up to seven “land units” including three urban density types as well as natural vegetation, crop, glacier and lake. The CLMU5 is a single-layer urban canopy model within CTSM that serves as the urban land parameterization for the three urban land units. An urban land unit is composed of five facets: roof, sunlit wall, shaded wall, previous and impervious surfaces on the canyon floor. These urban facets are arranged in an urban canyon configuration (Figure 2a).

A present-day global urban extent and urban properties dataset was originally developed for CESM by Jackson et al. (2010) and subsequently updated in CLMU5 (Oleson & Feddema, 2020). The spatial extent of urban areas is derived from a population density dataset at 1-km spatial resolution. Each urban pixel is classified as one of the four urban density classes: tall building district (TBD), high density (HD), medium density (MD), and low density (LD). The three urban land units corresponding to TBD, HD, and MD classes are used in current CLMU, which represent city core, commercial/industrial, and residential areas, respectively. The LD class is currently not used because these areas tend to be very sparsely built (i.e., closer to a rural setting) and seem to be better simulated using a vegetation model. Present-day urban morphological (e.g., building height, street width, pervious ground fraction), thermal (e.g., heat capacity and thermal conductivity), and radiative (e.g., albedo and emissivity) properties as well as building interior maximum and minimum thermostat settings (cooling and heating setpoint temperatures, respectively) that control the need for HAC are derived (see Figure 1 in Oleson & Feddema, 2020) from a variety of data sources such as local building codes, municipal documentation and published construction data and validated against Google Earth imagery (Jackson et al., 2010). They can be defined uniquely for thirty-three regions of similar physical and social characteristics spanning the global land surface and for each density class (see Jackson et al., 2010 and Oleson & Feddema, 2020 for details). The CLMU has been evaluated against remote sensing and in-situ observations across the globe (Demuzere et al., 2008, 2014, 2017; Demuzere et al., 2013; Fitria et al., 2019; Karsisto et al., 2016; Lin et al., 2016;

Mohammad Harmay & Choi, 2022; Oleson et al., 2008; Oleson & Feddema, 2020; Zhao et al., 2014, 2021).

The BEM in CLMU is a simplified dynamic model that can operate globally with sufficient accuracy and within the constraints of available global urban surface data. For each urban density type in every grid cell that has an urban area, an “average building” is simulated to represent buildings in that area, with specified geometric, radiative, and thermal properties based on the CLMU global surface dataset. Processes that are accounted for in the BEM include heat conduction through building surfaces (roof, sunlit and shaded walls, and floor), convection (sensible heat exchange) between interior surfaces and indoor air, longwave radiation exchange between interior surfaces, and ventilation (natural infiltration and exfiltration) (Figure 2a). Solar heat gain through windows due to direct solar radiation is neglected in the current version due to a lack of global data, but the effects of windows on the overall heat transfer properties of walls are accounted for. The heat storage by internal construction materials and internal heat gains from appliances and occupants are also not parameterized in the current version of the CLMU. These factors imply a possible overestimation of heating and underestimation of air-conditioning energy demand.

Space air-conditioning (heating) energy demand can be directly output from the BEM and calculated as the amount of energy flux required to be removed (added) to bring the interior building temperature down (up) to the cooling (heating) setpoint temperature. The BEM assumes a single thermal zone and infinite-capacity HAC systems. This

means the system supplies the amount of energy needed to keep the indoor air temperature within the specified limits at the time step of the model.

HAC adoption rates are implicitly modeled by the space heating and cooling setpoints (hereinafter referred to as proxy setpoints), defined by the urban dataset for each global region and urban density class. Using AC as an example, regions with higher AC adoption rates have lower AC proxy setpoints that are closer to what the thermostat settings would be in an actual building. Having a higher proxy setpoint would mean that the air conditioners only work during hotter time periods, which approximates having fewer air conditioners in an urban area (Figure 2a and c). As a result, the AC proxy setpoints in the original dataset have a large range that spans 27 to 42°C (Oleson & Feddema, 2020).

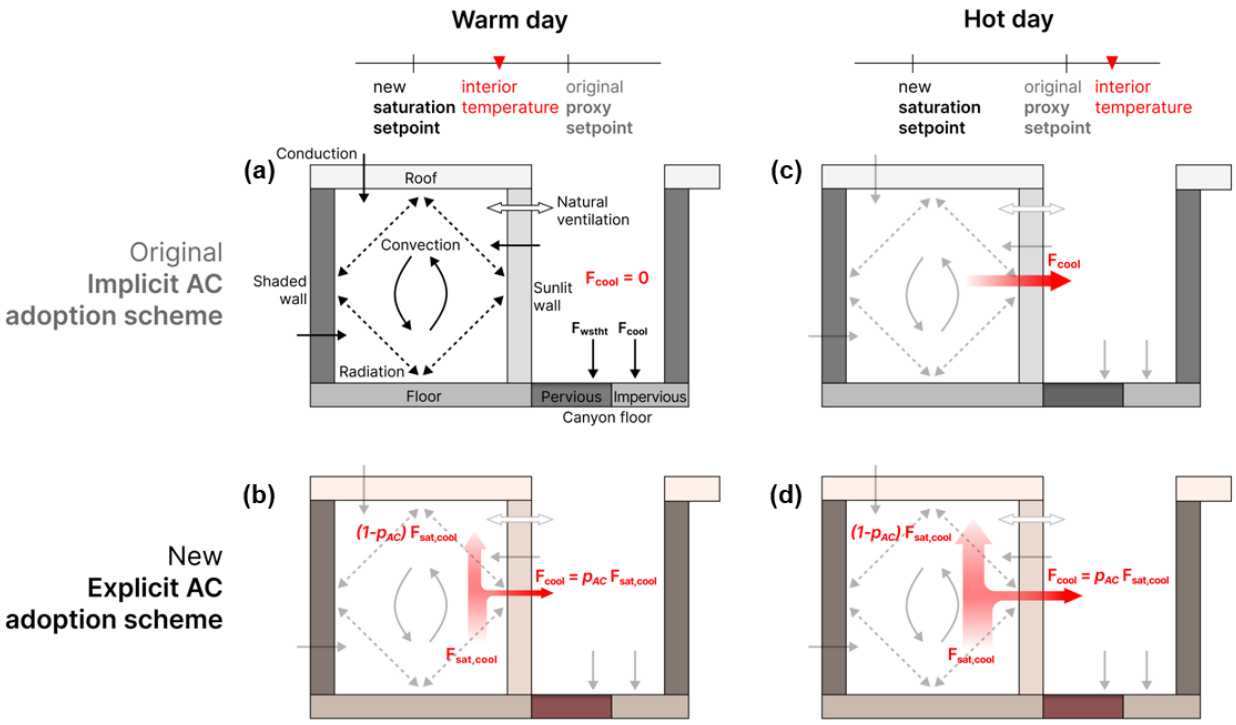

Figure 2. Schematic diagrams of current implicit-AC-adoption (a, c) and new explicit-AC-adoption (b, d) modeling schemes on an illustrative warm day (a, b) and an illustrative hot day (c, d) for a place of relatively low AC adoption. Surfaces in the urban canyon and processes simulated by the BEM are labeled in (a). The sizes of arrows in (d) are larger than those in (b) to indicate more AC energy flux is produced on a hot day. The fluxes in the building interior in (b) and (d) are used to update the interior building temperature after each time step (see Section 3). F_{cool}, AC energy flux. F_{wstht}, losses from inefficiencies in the HAC equipment and in the conversion of primary to end use energy. They are returned as sensible heat to the canyon floor and distributed to both pervious and impervious surfaces. $F_{sat,cool}$, AC energy flux under saturated AC adoption. p_{AC}, AC adoption rate.

3. Mathematical model for explicit-AC-adoption scheme

Currently, AC adoption rate can be modeled in the BEM embedded in regional-scale climate models such as the Weather Research and Forecasting model. That BEM is more detailed and allows control for individual building's AC setpoints schedules (e.g., AC will only work during business hours in office buildings) (Salamanca et al., 2009), so AC adoption can be controlled by turning on/off each building's HAC system. However, representing and controlling each individual building is usually neither feasible nor necessary for global-scale climate models or ESMs. We hence propose an explicit-AC-adoption scheme in CLMU that characterizes AC adoption at each grid cell with an adoption rate parameter, as illustrated in Figure 2b and d and described below.

Under the original scheme, the AC flux, F_{cool} , at each time step is calculated as:

$$F_{cool} = \frac{H\rho C_p}{\Delta t} \left({T_{i_B}}^t - T_{max}\right), for\ {T_{i_B}}^t > T_{max};$$

$$= 0, otherwise, \quad (1)$$

where H is building height, ρ is air density, C_p is the specific heat of dry air, Δt is the timestep of the model simulation, T_{i_B} is the interior building temperature, T_{max} is the AC proxy setpoint, and t denotes the timestep. If F_{cool} is not zero, the indoor air temperature at the next is then reset to T_{max}:

$${T_{i_B}}^{t+1} = T_{max}. \quad (2)$$

In the proposed new explicit-AC-adoption paramterization scheme, we add an explicit AC adoption rate parameter, p_{AC}, to the current calculation of AC flux. We first calculate the AC flux under saturated AC adoption (i.e., p_{AC} = 100%):

$$F_{sat,cool} = \frac{H\rho C_p}{\Delta t}\ ({T_{i_B}}^t - T_{sat,max}\ ), for\ {T_{i_B}}^t > T_{sat,max};$$

$$= 0, otherwise \quad (3)$$

where $T_{sat,max}$ is the AC setpoint when the AC adoption is saturated. The actual AC flux being removed from the indoor air is then scaled based on the adoption rate:

$$F_{cool} = p_{AC} \cdot F_{sat,cool} \quad (4)$$

The interior building temperature is then reset as follows:

$${T_{i_B}}^{t+1} = \frac{(1 - p_{AC})\ F_{sat,cool}\ \Delta t}{H\rho C_p} + T_{sat,max} \quad (5)$$

The anthropogenic heat added to the urban canyon due to AC energy use, $F_{wstht,AC}$, is calculated as:

$$F_{wstht,AC} = w_{AC} \cdot p_{AC} \cdot F_{sat,cool}, \quad (6)$$

where w_{AC} is the waste heat factor for AC, determined by the AC equipment coefficient of performance (COP_{AC}) and the weighted energy conversion efficiency ($P_{eff,cool}$) from primary to end use energy. The calculation and assumptions for w_{AC} remains unchanged from the original scheme as follows:

$$w_{AC} = \frac{1}{COP_{AC} \cdot P_{eff,cool}}, \quad (7)$$

Given the default values for COP_{AC} and $P_{eff,cool}$ in CLMU, w_{AC} is approximated as 0.6 globally (Oleson & Feddema, 2020).

4. New global AC adoption rate data

To support the new explicit AC adoption parameterization scheme, a global, spatially explicit dataset on the new variable, AC adoption rate (p_{AC}), is needed. There is limited AC adoption rate data available in the literature (Davis et al., 2021), as such data are

307 derived from household-level energy consumption surveys, which are usually conducted
308 by more affluent countries (Zheng et al., 2014). Substantial efforts are needed to
309 identify, locate, and access such survey results from various government agencies
310 across countries. In this study, we compile present-day AC adoption rate data (loosely
311 defined as between the years of 2010 and 2020) from sources such as International
312 Energy Agency (IEA), national surveys, scientific literature, and others (see Table S1),
313 and construct a global, spatially explicit AC adoption rate dataset at country- and sub-
314 country-level that works with CTSM. The new dataset is publicly available in tabular,
315 geospatial, and gridded formats for use in other Earth system modeling, energy
316 modeling, socioeconomic analyses, or integrated assessment applications.
317
318 We first collect residential AC adoption rate data from 35 countries (Table S1) which are
319 directly used in the dataset. These countries provide representative samples of the
320 world's countries that cover roughly 53% global land area, 68% of world population, and
321 70% of global Gross Domestic Product (The World Bank, 2023). To obtain global
322 coverage, we utilize the number of AC units per household data available from IEA
323 (Table S1) that covers 195 countries/regions, and derive a linear model with saturation
324 effect (two-segment piecewise linear fit) between AC adoption rate and number of AC
325 units per household for 34 common countries/regions where both quantities are
326 available. The linear model assumes that the line passes through the origin, and over a
327 certain number of AC units per household (saturation point), AC adoption rate does not
328 change as the number of AC units per household increases. The saturation point is
329 determined by minimizing the root mean squared error (RMSE) between the true and

fitted values ($r^2 = 0.89$, $p < 0.001$) (Fig. S1). Other factors, such as house/household size and income inequality, may help explain additional variations, but the simplified model allows us to obtain reasonably accurate AC adoption rate data for the majority of global countries/regions with the available information.

For countries where more detailed data are available, such as the United States, Australia, and China, the dataset also contains state- or province-level AC adoption rate data, collected or derived from the statistics released by the respective country's government agency (Table S1), to better represent the heterogeneity in these countries spanning highly diverse climate zones. State-level AC adoption rate data for the United States and Australia are available from their respective national surveys and are directly used. For China, data are available on the number of AC units per 100 households per province. The same linear model with saturation effect derived from the 34 countries/regions is applied to obtain province-level AC adoption rate data.

The tabular AC adoption rate data are then combined with shapefiles of global countries/regions and gridded to CTSM grids to produce the spatially explicit AC adoption rate dataset, as presented in Figure 3a-c. Since all data curated are from the residential sector, we assign the derived dataset to the MD urban density class that represents residential areas (Figure 3a). Under the assumption that most TBD classes, which represent city cores, are affluent commercial districts that universally utilize space cooling regardless of the socioeconomic status of the country they are in, we assign AC adoption rate of 1 to all TBD classes globally (Figure 3c). Note that TBD classes are

only present in 149 out of 4421 urban grid cells under the nominal grids and represent <1% of grid area. We then assign the simple average of the AC adoption rates from TBD and MD classes to the HD class of each country/region to represent the commercial/industrial areas that are transitional from central commercial to residential areas (Figure 3b).

For the missing countries, regions, and grid cells, we perform grid-cell-based nearest neighbor gap filling as detailed in the Supporting Information. This procedure follows the assumption that locations close to each other are likely to have similar climates, socioeconomic conditions and/or cultural preferences towards air conditioners. This allows us to obtain a complete global land coverage that is required by CTSM to perform simulations. The filled dataset is presented in Figure 3d-f.

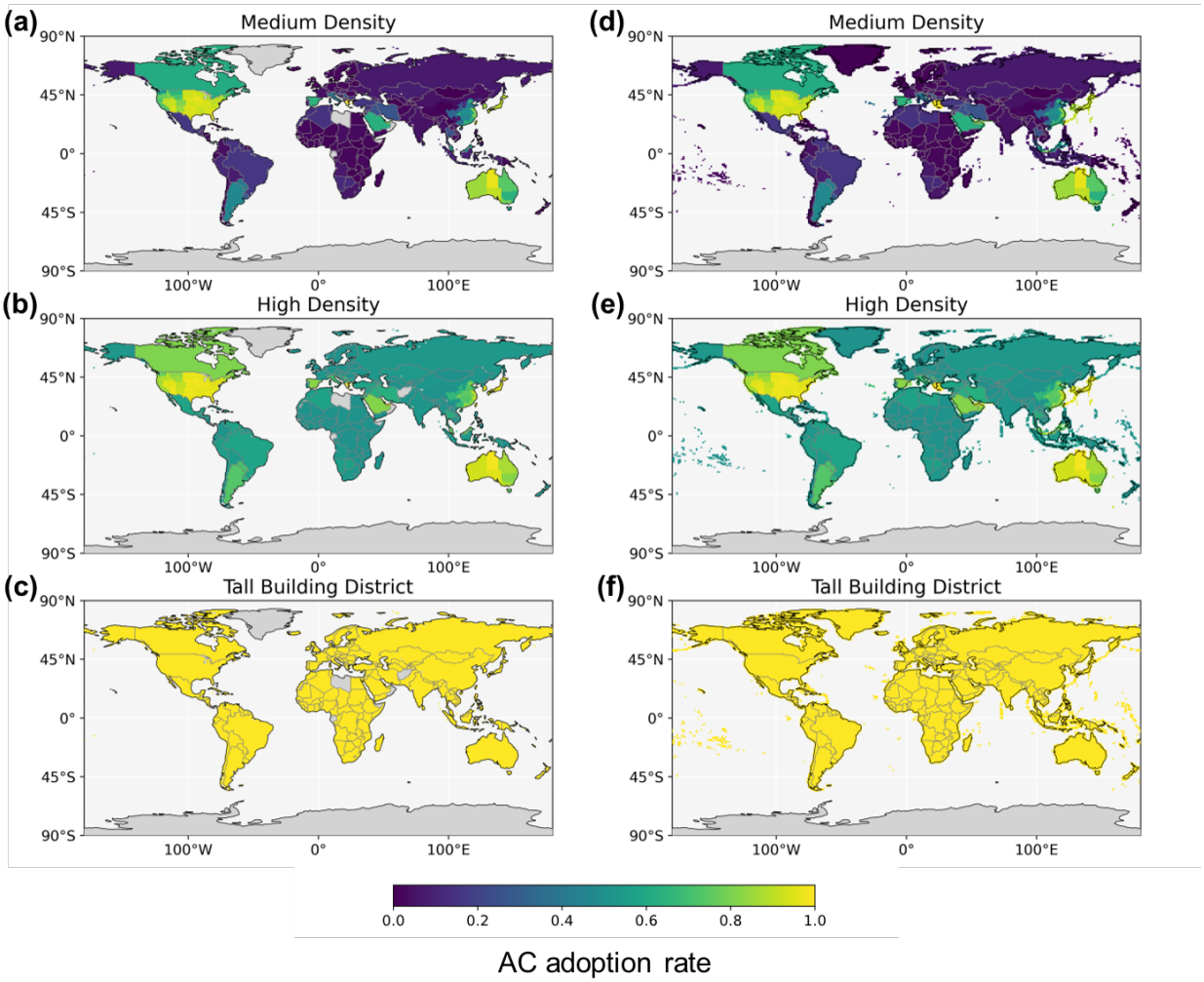

Figure 3. AC adoption rate in Tall Building District (TBD), High Density (HD) and Medium Density (MD) before (a-c) and after (d-f) gap filling. Shown at a spatial resolution of 0.9375° latitude ×1.25° longitude, the nominal resolution used by CESM for global simulations.

We provide both gridded and vector files of the original (before gap filling) data to support different modeling resolution or configuration requirements. The dataset also contains a quality control band that denotes the sources of the data and the associated level of confidence, to help classify the uncertainties in the dataset. We generate the

gap-filled AC adoption rate data in various resolutions for CTSM applications (latitude × longitude: 0.23° × 0.31°, 0.47° × 0.63°, 0.9375° ×1.25°). The dataset compiled for this work, both before and after gap filling, is freely available to the public for use in other Earth System Models aiming to better parameterize urban building energy, or other analyses that may benefit from country- or sub-country-level AC adoption rate information. Users are welcome to adopt the same gap filling procedure or apply a new one that better serves their needs.

Since the AC proxy setpoints in the original parameterization also implicitly represent AC adoption rates, they need to be changed under the explicit AC adoption modeling scheme so as to represent only building interior setpoints that more closely resemble realistic building thermostat settings. We use 27°C, the lowest AC setpoint in the original data which was applied to all three density classes in the southeast U.S., and apply it to all three density classes globally. This is because the southeast U.S. has one of the highest, and near-saturated AC adoption rates in the world under the AC adoption rate dataset (88% - 96% for MD), which offers a good reference point for the AC saturation behavior in the model. The setpoints can easily be changed when better AC setpoints datasets become available.

5. Simulations and validation

We perform a suite of global land-only simulations (i.e., the CTSM is active, while other components of CESM such as atmosphere, ocean, and sea ice use prescribed data) at 0.9375° latitude ×1.25° longitude spatial resolution to examine the effects of the explicit-

AC-adoption scheme and the spatially explicit AC adoption rate dataset. Simulations are run from 2000 - 2014 driven by atmospheric forcing (precipitation, incoming solar and longwave radiation, and air temperature, humidity, wind, and CO_2 concentration at the lowest atmospheric model layer) from the Global Soil Wetness Project forcing dataset (GSWP3) (http://hydro.iis.u-tokyo.ac.jp/GSWP3/). A control simulation (IMP_AC) is run with the original, implicit AC adoption parameterization scheme and the proxy AC thermostat setpoints. Four test simulations are run using the explicit-AC-adoption parameterization scheme: one with the global, spatially explicit AC adoption rate dataset (EXP_AC), and three additional ones with AC adoption rate set to 1 (EXP_AC_1), 0.03 (EXP_AC_TINY), and 0 (EXP_AC_0) everywhere for all three urban density classes. We focus on analyzing monthly average values of urban temperature and AC energy demand.

The urban extent (i.e., percent urban area in a grid cell) used in this study is derived from the historical urban land cover of year 2000 at 1-km resolution as presented in Gao & O'Neill (2020), which is based on Landsat remote sensing data. The urban extent dataset is then combined with the urban properties dataset described in Section 2, aggregated to the desired resolution (0.9375° latitude ×1.25° longitude in this study), and assigned urban density classes to produce the input data used by the model. Details on how the surface dataset is generated can be found in Fang et al. (2023).

We validate the explicit-AC-adoption scheme simulated AC energy demand with published, observation-based datasets by Varquez et al. (2021) and Flanner (2009) on

anthropogenic heat flux (AHF). The Flanner (2009) dataset is derived from country-specific data of energy consumption from non-renewable sources (coal, petroleum, natural gas, and nuclear), population density and national boundary data for year 2005. The Varquez et al. (2021) dataset uses the energy consumption data for the 2010s from the Shared Socioeconomic Pathways (SSP) framework, the energy balance statistics from IEA, and adjusted AHF distribution with nightlight satellite imagery. To obtain AHF due to AC, we collect AC energy use and total primary energy consumption data and derive an AC energy fraction (f) for each country/region where the required data are available (see Supporting Information). While total primary energy consumption data are readily available for most countries/regions, AC energy consumption data are sparse, which limits the coverage of possible f data. By leveraging publicly available datasets from the IEA and U.S. Energy Information Administration, we are able to obtain required data and calculate f for 14 countries/regions and 50 U.S. states. We then multiply these fractions with the AHF data to obtain estimates of AHF due to AC. The validation results are shown in Figures 4-6 and S2-4, and discussed in Section 6 below.

6. Results and Discussions

6.1 Improved modeling of AC energy flux in CLMU

The new explicit-AC-adoption parameterization and dataset improve the performance of AC energy flux simulation both in magnitude of AHF due to AC and in spatial variability. For the 14 countries/regions and 50 U.S. states where AHF due to AC energy use can be calculated (see Section 5 above and Supporting Information), the total annual AHF from AC is 0.12 TW (Figure 4c) in the EXP_AC run, whereas the IMP_AC run produces

445 0.04 TW (Figure 4c). This underestimation is due primarily to the effective AC adoption
446 rate in the original dataset being lower than the real-world values (Oleson & Feddema,
447 2020). The explicit AC adoption scheme and dataset are able to improve the
448 underestimation, and increase the total annual AHF due to AC to 0.08 TW. The spatial
449 correlation between the modeled results and the observations are also improved from
450 0.38 to 0.58.

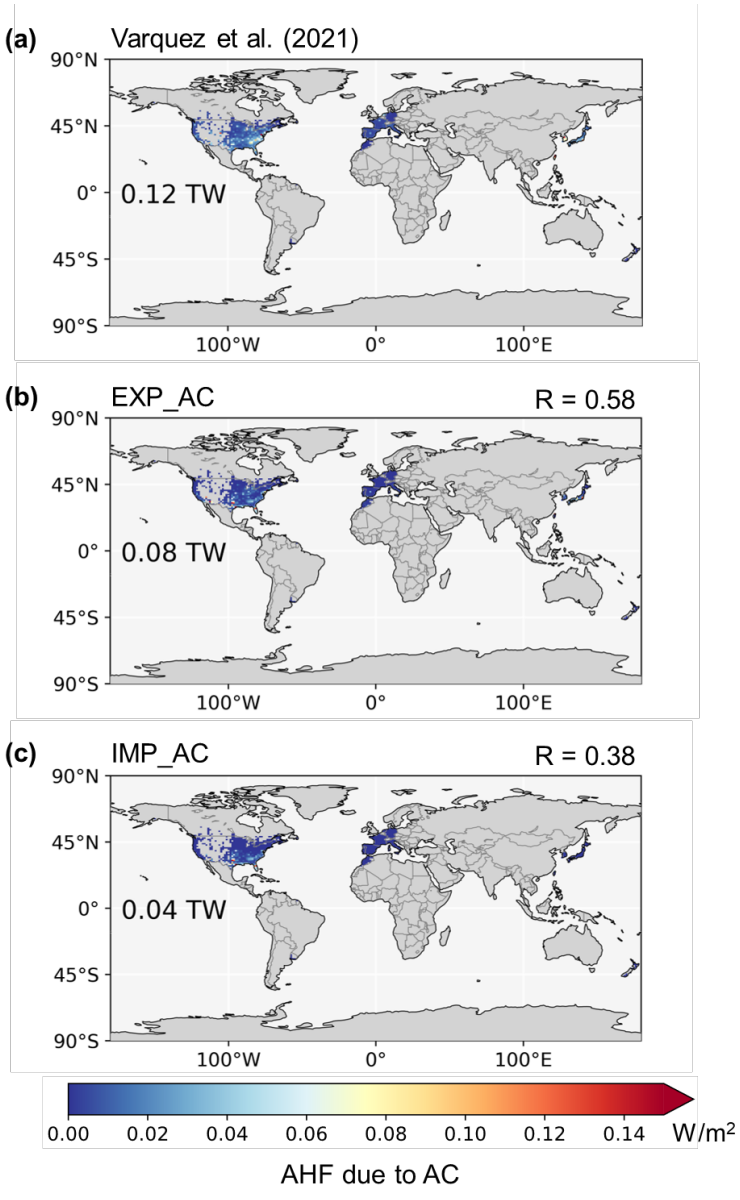

451

Figure 4. Improvements in modeled anthropogenic heat flux due to AC for available countries/regions in 2010 - 2014. (a) observational estimates derived from Varquez et al., (2021), (b) modeled AHF due to AC using the new explicit-AC-adoption scheme (EXP_AC), and (c) modeled AHF due to AC in using the original implicit-AC-adoption scheme (IMP_AC). Numbers in panels represent the total anthropogenic heat plotted in each panel. R is the pattern correlation between each panel and panel (a).

The performance improvements are also visible regionally. The total AHF due to AC in contiguous U.S. and parts of Canada increased from 0.04 TW (Figure 5c) to 0.06 TW (Figure 5b), as compared to 0.09 TW (Figure 5a) in the validation data. The spatial correlation between modeled and observed AHF also improved from 0.41 to 0.57, with most significant improvements in the north and southwest parts of the contiguous U.S. Major urban centers like New York, Chicago, Minneapolis, San Francisco, and Los Angeles had near-zero AC-induced AHF release in the IMP_AC run under the original scheme, and become clearly discernible under the explicit AC adoption scheme. For some European and North African countries (Figure 6a-c), the new scheme increased the annual total AHF due to AC from 0 (Figure 6c) to 0.003 TW (Figure 6b), as compared to the observational estimates of 0.01 TW (Figure 6a). The original scheme estimates all grid cell to be near-zero in AC use, and does not capture the spatial variations of the observations (spatial correlation $R = -0.07$). The explicit AC adoption scheme is able to capture some of the variations ($R = 0.28$) in Italy and south Spain, and of large urban centers such as Madrid and Paris. There seems to be an overestimation in Morocco's AHF from AC energy use under the explicit-AC-adoption

scheme, likely due to the assumptions made in urban thermal and radiative properties in the model. The AHF performance in Japan (Figure 6d-f) under the explicit-AC-adoption scheme is the best and the most improved among all regions, both in total AHF and the spatial correlations. The explicit AC adoption scheme improved the estimate of total AHF due to AC from 0 (Figure 6f) to 0.006 TW (Figure 6e), very close to the observational estimate of 0.008 TW (Figure 6d). The spatial correlation is improved from 0.17 to 0.92, suggesting most of the spatial variations can now be captured by the explicit AC adoption scheme. In general, the modeled AHF varies in a larger range than the observational estimates. While we acknowledge the possible limitations and assumptions of the model, another possible cause for the discrepancies stems from the use of nightlights in observational estimates of the AHF. The total energy consumption is distributed spatially by population and adjusted based on nightlight intensity (Varquez et al., 2021). This approach is subject to saturation effect (on high light intensity) and detection limit (on low light intensity) (M. Zhao et al., 2019), which can be reflected as smaller extremes in AHF variations than in reality.

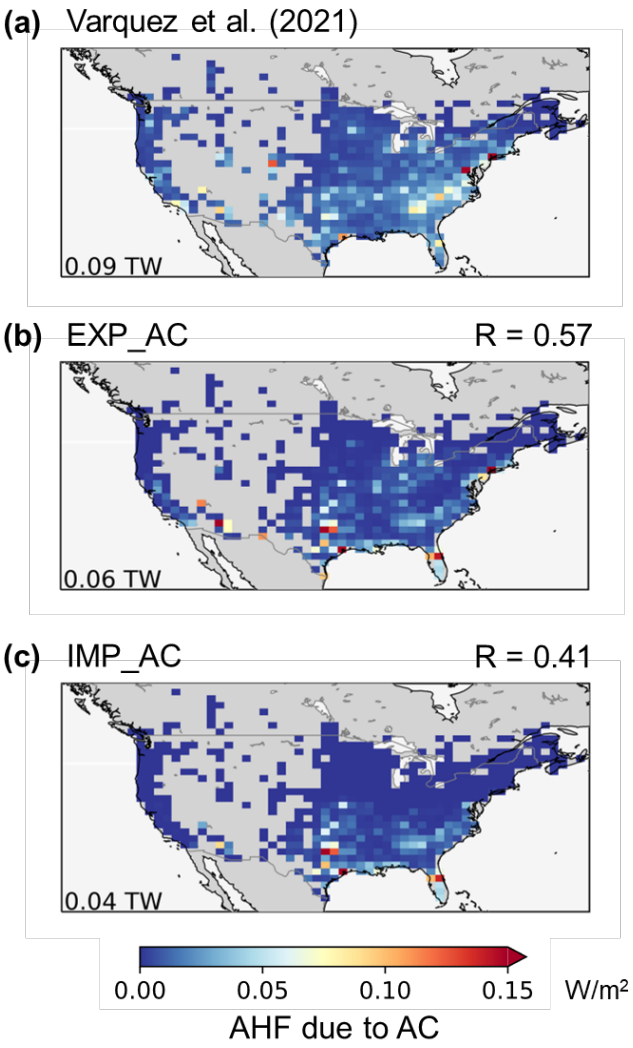

491

492 **Figure 5.** As in Figure 4 but for Contiguous US and parts of Canada.

493

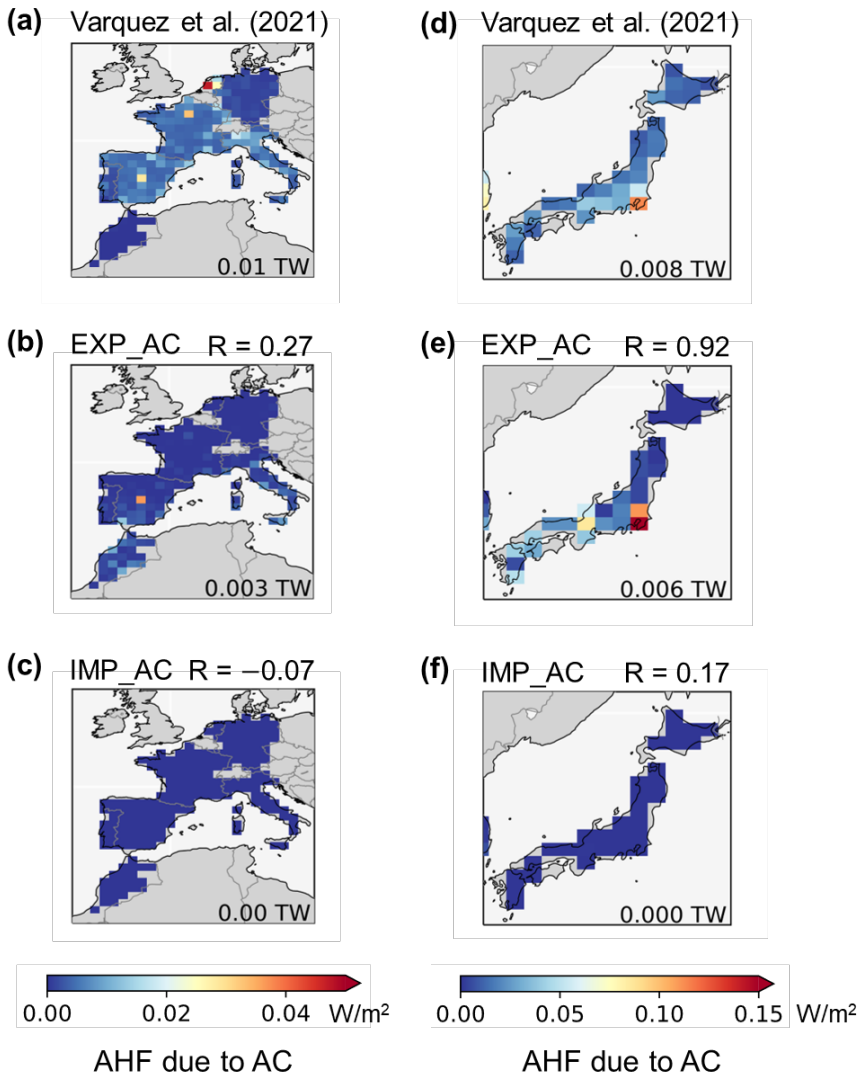

Figure 6. As in Figure 4 but for (a-c) Europe and North Africa, and (d-f) Japan.

6.2 Effects on other urban climate variables

We compare results for other urban climate variables including urban 2-meter air temperature, AC and heating energy flux, and waste heat flux, to illustrate the effects of the explicit-AC-adoption scheme and the AC adoption rate dataset. Comparing EXP_AC with IMP_AC, the global mean urban 2-meter air temperature does not change, but some regions are shown to experience slight temperature increase, such

as in the Middle East, Indian Peninsula, Middle America, and Southeast Asia (Figure 7a). This is a result of waste heat flux increase in these regions (Figure 7b), totaling 0.37 TW globally. The waste heat flux increase is driven by AC energy flux increase in the same areas (Figure 7c), as evidenced by the geospatial correlation between Figure 7b and 7c. Heating energy flux is essentially unchanged, with minimal decrease in the Midwest in the U.S. and Central-Eastern China (Figure 7d). These regions have an increased waste heat flux in the urban environment due to an increase in AC energy flux, thus requiring less heating during large diurnal temperature variations when both AC and heating energy fluxes are produced within a short period of time. This is due to the limitation that there is no seasonal schedule in the model which precludes AC or heating use from one another, whereas in reality, either AC or heating system in a building is usually active at a given time, not both. Note that the most substantial decrease in heating energy flux is about three orders of magnitude smaller than the usual heating energy flux during heating seasons, suggesting that the decrease is trivial.

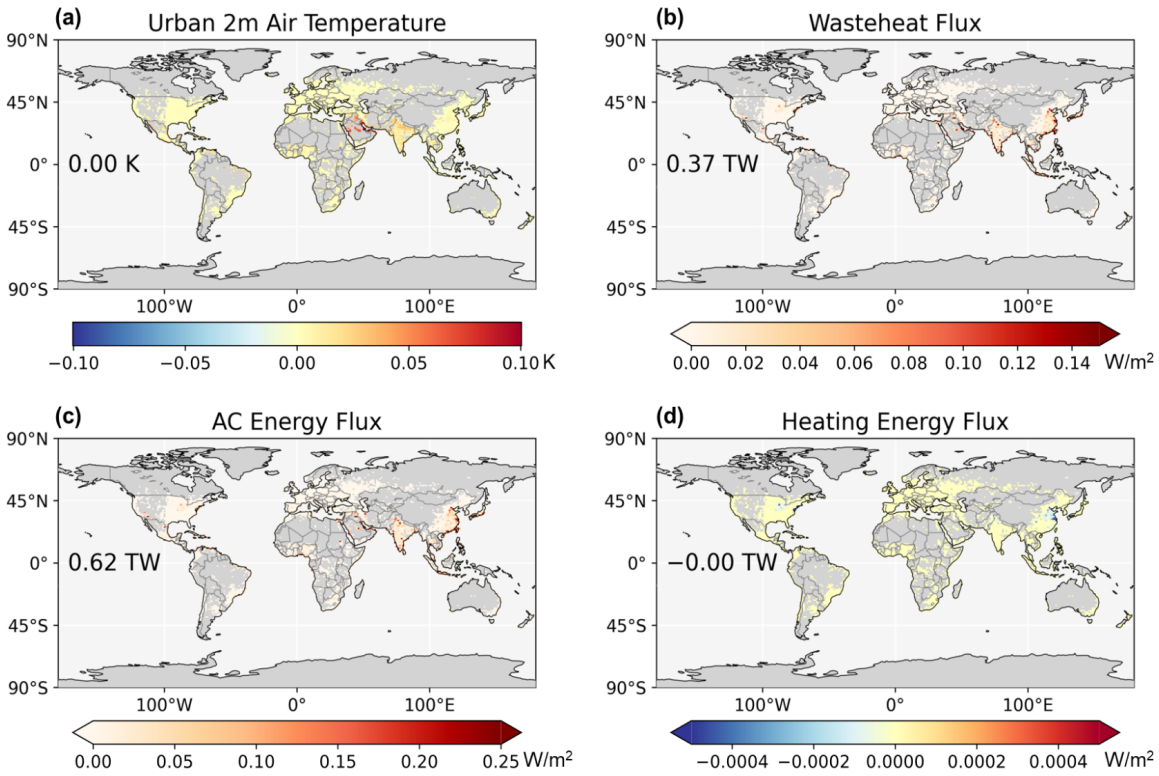

Figure 7. Mean differences between the results from the new explicit-AC-adoption scheme (EXP_AC) and the original implicit-AC-adoption scheme (IMP_AC) on (a) urban 2-meter air temperature, (b) waste heat flux, (c) AC energy flux, and (d) heating energy flux, for 2005 - 2014. The number in (a) represents the area-weighted global mean, and numbers in (b-d) represent the global total differences.

6.3 New capabilities of the explicit-AC-adoption scheme

The new explicit-AC-adoption scheme makes it possible to conduct global-scale experiments using CTSM on the effects of AC adoption on urban energy and climate through dynamic modeling. We conduct three experiments under the present-day climate for idealized (100% adoption, EXP_AC_1), very low (3%, EXP_AC_TINY), and zero AC adoption (EXP_AC_0), and compare them with the result from the EXP_AC run

where present-day AC adoption rates are used. Compared with the current world under the present-day adoption rates, an idealized world where AC adoption is saturated (100%) everywhere would mean a drastic increase in AC adoption for warmer climates and less affluent regions such as most of Africa, Middle and South America, Central Asia, India, and Southeast Asia, as well as in cooler climates such as most of Europe, New Zealand, and Northern Asia (Figure 8a). The increase in AC adoption does not translate equally to an increase in AC energy flux in all regions (Figure 8d). AC energy flux increase is concentrated around Central Africa, India, and Southeast Asia, as the warmer present-day climates in these regions mean that AC use can be easily triggered, thus highlighting the effect of saturated AC adoption. We can expect that the effect of saturated AC adoption will become more pronounced in the future under climate change for currently cooler regions, where higher summer temperatures may necessitate the use of AC. The increase in AC energy flux causes an average regional warming of up to 0.09 K (Figure 8g). Under a very low adoption rate scenario, most countries would have a lower AC adoption rate than present day, with the U.S., Japan, South Korea, coastal regions of China, Australia, and Greece having the largest differences (Figure 8b). Some regions (white in Figure 8b) currently have AC adoption rates lower than 3%, which means their adoption rates are increased in this scenario, albeit minutely. The AC energy flux differences are the most pronounced for regions with the largest adoption rate differences, but are also prominent around the Middle East, India, and Southeast Asia, despite only a minor difference in adoption rate between the two scenarios (2% increase in the case of India) (Figure 8e). This means that even minor increases in AC adoption rate in these regions could lead to

554 substantially more AC energy use. Moreover, the temperature differences induced by
555 the higher AC energy flux are higher in these regions (Figure 8h), even when the AC
556 flux differences are on the same order of magnitude as those with the highest adoption
557 rate differences. This suggests that not only is the AC energy flux in these regions more
558 sensitive to AC adoption rate change, but their urban temperature is also more sensitive
559 to anthropogenic heat than in other regions. Comparing the very low adoption rate
560 scenario with the no-AC scenario, most of the regions show marginal differences in AC
561 energy flux or urban temperature, except for a few spots visible around the equator.
562 These experiments demonstrate that the explicit-AC-adoption scheme opens doors to
563 further investigation into urban climate-energy feedbacks, and sets up the groundwork
564 for incorporating AC adoption rate changes due to climate change and socioeconomic
565 development in CESM's future energy and climate projections.

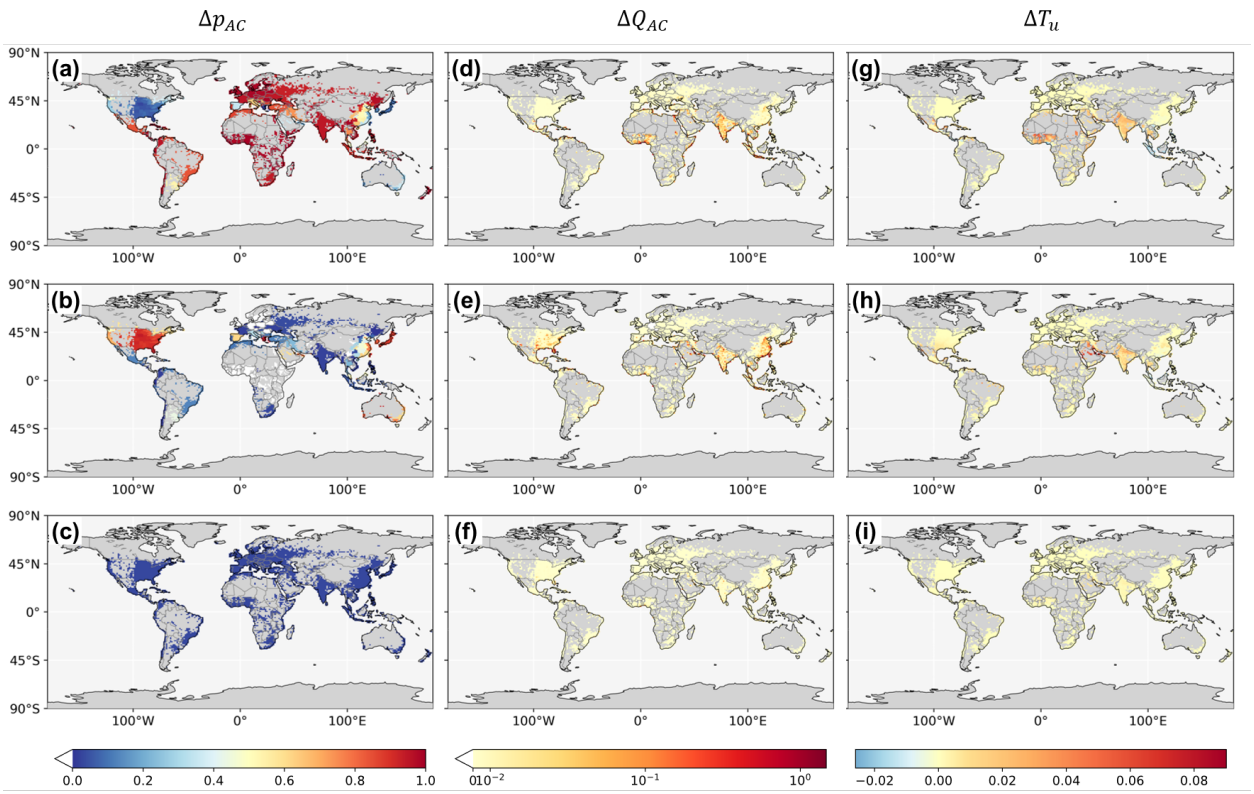

Figure 8. Mean differences in (a-c) AC adoption rate (showing medium density), (d-f) monthly mean AC energy flux, and (g-i) monthly mean urban 2-meter air temperature between the results from (a, d, g) idealized adoption (100%, EXP_AC_1) and current adoption (EXP_AC), (b, e, h) current (EXP_AC) and very low adoption (3%, EXP_AC_TINY), and (c, f, i) very low (EXP_AC_TINY) and no adoption (EXP_AC_0), for 2005 - 2014.

7. Conclusions

The CLMU in CTSM is one of the few dynamic urban parameterizations in ESMs with a fully coupled, physics-based building energy model. Despite its recent development and improvement in performance, a critical limitation still remains, where AC adoption is modeled implicitly with the use of proxy interior building thermostat setpoints. This

undermines the physical interpretability of the model, poses challenges for ensuring model accuracy, limits the model's capability in integrating socioeconomic and climate change impact on urban energy, and hinders inter-model and inter-regional climate risk assessments. In this work, we establish a new explicit AC adoption parameterization scheme by adding an AC adoption rate parameter. This scheme separates building thermostat setpoint and AC adoption rate into independent parameters that can be tuned separately. In support of the new scheme, we develop a present-day global spatially explicit AC adoption rate dataset for use in CTSM and that can be leveraged in other climate and energy modeling applications and socioeconomic or integrated assessment analyses.

The explicit-AC-adoption parameterization scheme and the global AC adoption rate dataset significantly improve the CTSM's performance in modeling building AC energy flux, both in magnitude and spatial variability. The new scheme makes it possible to conduct global-scale experiments on the effects of changing AC adoption rate that help reveal the inter-regional differences in urban energy-climate feedbacks. These developments help improve the climate simulations and enhance CESM's ability to simulate urban energy use in response to and affecting local to regional climate. Although these developments are implemented in CTSM, the concept, mathematical model, and the dataset could be easily adapted to other ESMs. This work represents a step forward in interlinking climate and energy modeling at a global scale and better representations of coupled human-urban-Earth dynamics in ESMs.

As urban areas garner increased attention in national and international climate impact, adaptation and vulnerability assessments (IPCC, 2022; Reidmiller et al., 2018), the new explicit-AC-adoption parameterization makes CESM a valuable tool in urban climate and energy assessmenta on a global scale. The explicit AC adoption scheme sets up the infrastructure for making global future projections of urban energy and climate under various climate and socioeconomic scenarios, e.g., the SSP-Representative Concentration Pathways (RCP) scenario framework. As a global-scale model, CESM can generate globally coherent results that enable inter-regional comparison and knowledge transfer. If coupled with other CESM components for dynamic, fully coupled simulations, CTSM would be able to reveal the indirect impacts of AC adoption rate changes on large-scale dynamics due to teleconnections that may be amplified under climate change, which cannot be achieved by regional or local scale models.

The new present-day AC adoption rate dataset constructed in this study fills the gap in the literature (Davis et al., 2021) by providing global coverage for AC adoption rate data. It could be leveraged in other ESMs for better parameterization of urban building energy use, as well as other large-scale models (such as Integrated Assessment Models) or analyses. It can be used to calibrate existing AC adoption rate models (such as in Isaac & van Vuuren, 2009) and as base values to project AC adoption rate under various SSP-RCP scenarios, using AC adoption rate models based on climate (mostly cooling degree days) and income (such as in Sailor & Pavlova, 2003, and McNeil & Letschert, 2010).

A few potential development pathways may further improve CTSM's performance in AC energy flux modeling. More intra-country AC adoption rate data and global building thermostat settings data could be readily incorporated when they become available. Improvements in the resolution and accuracy of the urban surface data, such as the urban radiative, thermal, and morphological properties, are expected to further improve the magnitude and spatial correlation of simulated anthropogenic heat due to AC.

Model and tools availability

The CTSM code used in this study is publicly available at [URL to be released upon publication]. It will be incorporated as part of a future release through the Community Terrestrial System Model (CTSM) git repository (https://github.com/ESCOMP/ctsm).

Data Availability Statement

The AC adoption rate data and simulation results are archived and publicly available at [URL and doi to be released upon publication].

Acknowledgments

L.Z. acknowledges the support by the U.S. National Science Foundation (CAREER Award Grant No. 2145362) and the Institute for Sustainability, Energy, and Environment at the University of Illinois Urbana-Champaign. We acknowledge the high-performance computing support from Cheyenne (https://doi.org/10.5065/D6RX99HX) provided by NCAR's Computational and Information Systems Laboratory, sponsored by the U.S. National Science Foundation. The authors declare no conflict of interest.

References

Allen, L., Lindberg, F., & Grimmond, C. S. B. (2011). Global to city scale urban anthropogenic heat flux: model and variability. *International Journal of Climatology*, *31*(13), 1990–2005. https://doi.org/10.1002/joc.2210

Colelli, F. P., & Cian, E. D. (2020). Cooling demand in integrated assessment models: a methodological review. *Environmental Research Letters*, *15*(11), 113005. https://doi.org/10.1088/1748-9326/abb90a

Craig, M. T., Wohland, J., Stoop, L. P., Kies, A., Pickering, B., Bloomfield, H. C., et al. (2022). Overcoming the disconnect between energy system and climate modeling. *Joule*. https://doi.org/10.1016/j.joule.2022.05.010

Creutzig, F., Baiocchi, G., Bierkandt, R., Pichler, P.-P., & Seto, K. C. (2015). Global typology of urban energy use and potentials for an urbanization mitigation wedge. *Proceedings of the National Academy of Sciences*, *112*(20), 6283–6288. https://doi.org/10.1073/pnas.1315545112

Davis, L., Gertler, P., Jarvis, S., & Wolfram, C. (2021). Air conditioning and global inequality. *Global Environmental Change*, *69*, 102299. https://doi.org/10.1016/j.gloenvcha.2021.102299

Davis, L. W., & Gertler, P. J. (2015). Contribution of air conditioning adoption to future energy use under global warming. *Proceedings of the National Academy of Sciences*, *112*(19), 5962–5967. https://doi.org/10.1073/pnas.1423558112

Demuzere, M., De Ridder, K., & Van Lipzig, N. P. M. (2008). Modeling the energy balance in Marseille: Sensitivity to roughness length parameterizations and

671 thermal admittance. *Journal of Geophysical Research: Atmospheres*, *113*(D16).
672 https://doi.org/10.1029/2007JD009113
673 Demuzere, M., Coutts, A. M., Göhler, M., Broadbent, A. M., Wouters, H., van Lipzig, N.
674 P. M., & Gebert, L. (2014). The implementation of biofiltration systems, rainwater
675 tanks and urban irrigation in a single-layer urban canopy model. *Urban Climate*,
676 *10*, 148–170. https://doi.org/10.1016/j.uclim.2014.10.012
677 Demuzere, M., Harshan, S., Järvi, L., Roth, M., Grimmond, C. S. B., Masson, V., et al.
678 (2017). Impact of urban canopy models and external parameters on the modelled
679 urban energy balance in a tropical city. *Quarterly Journal of the Royal*
680 *Meteorological Society*, *143*(704), 1581–1596. https://doi.org/10.1002/qj.3028
681 Demuzere, Matthias, Oleson, K., Coutts, A. M., Pigeon, G., & van Lipzig, N. P. M.
682 (2013). Simulating the surface energy balance over two contrasting urban
683 environments using the Community Land Model Urban. *International Journal of*
684 *Climatology*, *33*(15), 3182–3205. https://doi.org/10.1002/joc.3656
685 Deroubaix, A., Labuhn, I., Camredon, M., Gaubert, B., Monerie, P.-A., Popp, M., et al.
686 (2021). Large uncertainties in trends of energy demand for heating and cooling
687 under climate change. *Nature Communications*, *12*(1), 5197.
688 https://doi.org/10.1038/s41467-021-25504-8
689 Fang, B., Zhao, L., Oleson, K. W., Zhang, K., Lawrence, P. J., Sacks, B., et al. (2023,
690 June 14). Representing dynamic urban land change in the Community Earth
691 System Model (CESM). preprint, Preprints.
692 https://doi.org/10.22541/essoar.168676909.95382628/v1

693 Fitch, A. C. (2015). Climate Impacts of Large-Scale Wind Farms as Parameterized in a
694 Global Climate Model. *Journal of Climate*, *28*(15), 6160–6180.
695 https://doi.org/10.1175/JCLI-D-14-00245.1
696 Fitria, R., Kim, D., Baik, J., & Choi, M. (2019). Impact of Biophysical Mechanisms on
697 Urban Heat Island Associated with Climate Variation and Urban Morphology.
698 *Scientific Reports*, *9*(1), 19503. https://doi.org/10.1038/s41598-019-55847-8
699 Flanner, M. G. (2009). Integrating anthropogenic heat flux with global climate models.
700 *Geophysical Research Letters*, *36*(2). https://doi.org/10.1029/2008GL036465
701 Gao, J., & O'Neill, B. C. (2020). Mapping global urban land for the 21st century with
702 data-driven simulations and Shared Socioeconomic Pathways. *Nature*
703 *Communications*, *11*(1), 2302. https://doi.org/10.1038/s41467-020-15788-7
704 Güneralp, B., Zhou, Y., Ürge-Vorsatz, D., Gupta, M., Yu, S., Patel, P. L., et al. (2017).
705 Global scenarios of urban density and its impacts on building energy use through
706 2050. *Proceedings of the National Academy of Sciences*, *114*(34), 8945–8950.
707 https://doi.org/10.1073/pnas.1606035114
708 Hadley, S. W., Erickson III, D. J., Hernandez, J. L., Broniak, C. T., & Blasing, T. J.
709 (2006). Responses of energy use to climate change: A climate modeling study.
710 *Geophysical Research Letters*, *33*(17). https://doi.org/10.1029/2006GL026652
711 Hu, A., Levis, S., Meehl, G. A., Han, W., Washington, W. M., Oleson, K. W., et al.
712 (2016). Impact of solar panels on global climate. *Nature Climate Change*, *6*(3),
713 290–294. https://doi.org/10.1038/nclimate2843
714 Hurrell, J. W., Holland, M. M., Gent, P. R., Ghan, S., Kay, J. E., Kushner, P. J., et al.
715 (2013). The Community Earth System Model: A Framework for Collaborative

716 Research. *Bulletin of the American Meteorological Society*, *94*(9), 1339–1360.
717 https://doi.org/10.1175/BAMS-D-12-00121.1
718 Ichinose, T., Shimodozono, K., & Hanaki, K. (1999). Impact of anthropogenic heat on
719 urban climate in Tokyo. *Atmospheric Environment*, *33*(24), 3897–3909.
720 https://doi.org/10.1016/S1352-2310(99)00132-6
721 IPCC. (2022). Summary for Policymakers. In *Climate Change 2022: Impacts,*
722 *Adaptation, and Vulnerability. Contribution of Working Group II to the Sixth*
723 *Assessment Report of the Intergovernmental Panel on Climate Change* ([H.-O.
724 Pörtner, D.C. Roberts, M. Tignor, E.S. Poloczanska, K. Mintenbeck, A. Alegría,
725 M. Craig, S. Langsdorf, S. Löschke, V. Möller, A. Okem, B. Rama (eds.)]).
726 Cambridge University Press. Retrieved from
727 https://report.ipcc.ch/ar6wg2/pdf/IPCC_AR6_WGII_SummaryForPolicymakers.pd
728 f
729 Isaac, M., & van Vuuren, D. P. (2009). Modeling global residential sector energy
730 demand for heating and air conditioning in the context of climate change. *Energy*
731 *Policy*, *37*(2), 507–521. https://doi.org/10.1016/j.enpol.2008.09.051
732 Jackson, T. L., Feddema, J. J., Oleson, K. W., Bonan, G. B., & Bauer, J. T. (2010).
733 Parameterization of Urban Characteristics for Global Climate Modeling. *Annals of*
734 *the Association of American Geographers*, *100*(4), 848–865.
735 https://doi.org/10.1080/00045608.2010.497328
736 Karsisto, P., Fortelius, C., Demuzere, M., Grimmond, C. S. B., Oleson, K. W.,
737 Kouznetsov, R., et al. (2016). Seasonal surface urban energy balance and
738 wintertime stability simulated using three land-surface models in the high-latitude

city Helsinki. *Quarterly Journal of the Royal Meteorological Society*, *142*(694), 401–417. https://doi.org/10.1002/qj.2659

Kikegawa, Y., Tanaka, A., Ohashi, Y., Ihara, T., & Shigeta, Y. (2014). Observed and simulated sensitivities of summertime urban surface air temperatures to anthropogenic heat in downtown areas of two Japanese Major Cities, Tokyo and Osaka. *Theoretical and Applied Climatology*, *117*(1), 175–193. https://doi.org/10.1007/s00704-013-0996-8

Kikegawa, Y., Nakajima, K., Takane, Y., Ohashi, Y., & Ihara, T. (2022). A quantification of classic but unquantified positive feedback effects in the urban-building-energy-climate system. *Applied Energy*, *307*, 118227. https://doi.org/10.1016/j.apenergy.2021.118227

Lin, S., Feng, J., Wang, J., & Hu, Y. (2016). Modeling the contribution of long-term urbanization to temperature increase in three extensive urban agglomerations in China. *Journal of Geophysical Research: Atmospheres*, *121*(4), 1683–1697. https://doi.org/10.1002/2015JD024227

Mastrucci, A., van Ruijven, B., Byers, E., Poblete-Cazenave, M., & Pachauri, S. (2021). Global scenarios of residential heating and cooling energy demand and CO2 emissions. *Climatic Change*, *168*(3), 14. https://doi.org/10.1007/s10584-021-03229-3

McNeil, M. A., & Letschert, V. E. (2010). Modeling diffusion of electrical appliances in the residential sector. *Energy and Buildings*, *42*(6), 783–790. https://doi.org/10.1016/j.enbuild.2009.11.015

761 Mohammad Harmay, N. S., & Choi, M. (2022). Effects of heat waves on urban warming
762 across different urban morphologies and climate zones. *Building and*
763 *Environment*, *209*, 108677. https://doi.org/10.1016/j.buildenv.2021.108677
764 Oleson, K. W., & Feddema, J. (2020). Parameterization and Surface Data
765 Improvements and New Capabilities for the Community Land Model Urban
766 (CLMU). *Journal of Advances in Modeling Earth Systems*, e2018MS001586.
767 https://doi.org/10.1029/2018MS001586@10.1002/(ISSN)1942-2466.CESM2
768 Oleson, K. W., Bonan, G. B., Feddema, J., Vertenstein, M., & Grimmond, C. S. B.
769 (2008). An Urban Parameterization for a Global Climate Model. Part I:
770 Formulation and Evaluation for Two Cities. *Journal of Applied Meteorology and*
771 *Climatology*, *47*(4), 1038–1060. https://doi.org/10.1175/2007JAMC1597.1
772 Rastogi, D., Holladay, J. S., Evans, K. J., Preston, B. L., & Ashfaq, M. (2019). Shift in
773 seasonal climate patterns likely to impact residential energy consumption in the
774 United States. *Environmental Research Letters*, *14*(7), 074006.
775 https://doi.org/10.1088/1748-9326/ab22d2
776 Reidmiller, D. R., Avery, C. W., Easterling, D. R., Kunkel, K. E., Lewis, K. L. M.,
777 Maycock, T. K., & Stewart, B. C. (2018). *Impacts, Risks, and Adaptation in the*
778 *United States: The Fourth National Climate Assessment, Volume II*. U.S. Global
779 Change Research Program. https://doi.org/10.7930/NCA4.2018
780 van Ruijven, B. J., De Cian, E., & Sue Wing, I. (2019). Amplification of future energy
781 demand growth due to climate change. *Nature Communications*, *10*(1), 2762.
782 https://doi.org/10.1038/s41467-019-10399-3

783 Sailor, D. J., & Pavlova, A. A. (2003). Air conditioning market saturation and long-term
784 response of residential cooling energy demand to climate change. *Energy*, *28*(9),
785 941–951. https://doi.org/10.1016/S0360-5442(03)00033-1
786 Salamanca, F., Georgescu, M., Mahalov, A., Moustaoui, M., & Wang, M. (2014).
787 Anthropogenic heating of the urban environment due to air conditioning. *Journal*
788 *of Geophysical Research: Atmospheres*, *119*(10), 5949–5965.
789 https://doi.org/10.1002/2013JD021225
790 Salamanca, Francisco, Krpo, A., Martilli, A., & Clappier, A. (2009). A new building
791 energy model coupled with an urban canopy parameterization for urban climate
792 simulations—part I. formulation, verification, and sensitivity analysis of the model.
793 *Theoretical and Applied Climatology*, *99*(3), 331. https://doi.org/10.1007/s00704-
794 009-0142-9
795 Schaeffer, R., Szklo, A. S., Pereira de Lucena, A. F., Moreira Cesar Borba, B. S., Pupo
796 Nogueira, L. P., Fleming, F. P., et al. (2012). Energy sector vulnerability to
797 climate change: A review. *Energy*, *38*(1), 1–12.
798 https://doi.org/10.1016/j.energy.2011.11.056
799 Sharma, A., Wuebbles, D. J., & Kotamarthi, R. (2021). The Need for Urban-Resolving
800 Climate Modeling Across Scales. *AGU Advances*, *2*(1), e2020AV000271.
801 https://doi.org/10.1029/2020AV000271
802 Taseska, V., Markovska, N., & Callaway, J. M. (2012). Evaluation of climate change
803 impacts on energy demand. *Energy*, *48*(1), 88–95.
804 https://doi.org/10.1016/j.energy.2012.06.053

The World Bank. (2023). World Development Indicators [Data set]. Retrieved from https://databank.worldbank.org/source/world-development-indicators/preview/on

Varquez, A. C. G., Kiyomoto, S., Khanh, D. N., & Kanda, M. (2021). Global 1-km present and future hourly anthropogenic heat flux. *Scientific Data*, *8*(1), 64. https://doi.org/10.1038/s41597-021-00850-w

Wang, Y., Li, Y., Sabatino, S. D., Martilli, A., & Chan, P. W. (2018). Effects of anthropogenic heat due to air-conditioning systems on an extreme high temperature event in Hong Kong. *Environmental Research Letters*, *13*(3), 034015. https://doi.org/10.1088/1748-9326/aaa848

Wang, Y.-C., Bian, Z.-F., Qin, K., Zhang, Y., & Lei, S.-G. (2019). A modified building energy model coupled with urban parameterization for estimating anthropogenic heat in urban areas. *Energy and Buildings*, *202*, 109377. https://doi.org/10.1016/j.enbuild.2019.109377

Yalew, S. G., van Vliet, M. T. H., Gernaat, D. E. H. J., Ludwig, F., Miara, A., Park, C., et al. (2020). Impacts of climate change on energy systems in global and regional scenarios. *Nature Energy*, *5*(10), 794–802. https://doi.org/10.1038/s41560-020-0664-z

Zhao, L., Lee, X., Smith, R. B., & Oleson, K. (2014). Strong contributions of local background climate to urban heat islands. *Nature*, *511*(7508), 216–219. https://doi.org/10.1038/nature13462

Zhao, L., Oleson, K., Bou-Zeid, E., Krayenhoff, E. S., Bray, A., Zhu, Q., et al. (2021). Global multi-model projections of local urban climates. *Nature Climate Change*, 1–6. https://doi.org/10.1038/s41558-020-00958-8

Zhao, M., Zhou, Y., Li, X., Cao, W., He, C., Yu, B., et al. (2019). Applications of Satellite Remote Sensing of Nighttime Light Observations: Advances, Challenges, and Perspectives. *Remote Sensing*, *11*(17), 1971. https://doi.org/10.3390/rs11171971

Zheng, X., Wei, C., Qin, P., Guo, J., Yu, Y., Song, F., & Chen, Z. (2014). Characteristics of residential energy consumption in China: Findings from a household survey. *Energy Policy*, *75*, 126–135. https://doi.org/10.1016/j.enpol.2014.07.016

Supporting Information

Grid-cell-based nearest neighbor gap filling

To fill the missing countries and regions in the air-conditioning (AC) adoption rate (p_{AC}) dataset derived from the original data sources (Table S1), we perform grid-cell-based nearest neighbor gap filling with reference to the 33 regions in the original urban surface dataset (Jackson et al., 2010). The steps are described below.

1. Fill Greenland, which lies mostly in the arctic circle and is represented by a single region in the original dataset, with p_{AC} = 0.
2. Identify regions that contain a single country, and fill all missing grid cells in the region with that country's p_{AC} value. These countries include Brazil, Canada, India, and Russia.
3. Iterate through grid cells with missing values, starting from the southwest (bottom left) corner of the global map. Identify its four immediate neighbors: left, right, up, and down. Check whether a neighbor is filled (i.e., contains a value) in this order: left, right, down, and then up. As soon as a filled neighbor is encountered, assign the neighbor's value to the missing grid cell, and move on to the next missing grid cell. After this step, missing grid cells on the east coasts of the continents, and missing countries/regions with filled neighbors to the west are filled.
4. For the remaining grid cells with missing values, repeat Step 3 but start the iteration from the northeast (top right), and check the neighbors in this order instead: up, down, right, and then left. After this step, missing grid cells on the west coasts of the continents, and missing countries/regions with filled neighbors

to the east are filled. The remaining grid cells are islands isolated from the land mass.

5. All remaining missing grid cells in Japan are assigned Japan's p_{AC} value. This is a special handling step before the final sweep, due to the fact that the region Japan is part of contains also South Korea and North Korea, where the p_{AC} values vary between 0% and 91%. Assigning the median of this region would misrepresent the p_{AC} values of the islands in Japan.
6. Iterate through the 33 regions, and assign the median p_{AC} value of all available countries in each region to all missing grid cells in that region. We use median instead of mean to better represent the average behavior in regions with extreme (outlier) adoption rate values. We choose the median of all available countries, instead of all available grid cells in the region, to prevent the p_{AC} value being dominated by the countries of larger areas.

Deriving AC energy use fractions

The AC energy use fractions (f) are defined as the fraction of AC energy consumption over the total energy consumption for a given country/region. They are used to scale the total anthropogenic heat flux (AHF) data from Varquez et al. (2021) and Flanner (2009), which are based on total energy consumption in each country/region, to obtain the AHF due to AC used for validation in this study (Figures 4 - 6, and Figures S2 - S4). While total energy consumption data by country/region are readily available, AC energy consumption data are sparse, which limits the coverage of possible f data. By leveraging publicly available datasets from the International Energy Agency (IEA) and

U.S. Energy Information Administration (EIA), we are able to obtain required data and calculate f for 14 countries and 50 U.S. states using the methods detailed below.

Country-level data come from two free IEA datasets: 1) Energy Efficiency Indicators Highlights (EEI) (https://www.iea.org/data-and-statistics/data-product/energy-efficiency-indicators-highlights), which contains annual sectorial (residential, commercial, industry and transportation) and end-use final energy consumption (including AC energy consumption for residential and commercial sectors) for select countries; and 2) World Energy Balances Highlights (WEB) (https://www.iea.org/data-and-statistics/data-product/world-energy-balances-highlights), which contains annual total primary and final energy consumption for select countries. A total of 15 countries/regions (including the U.S.) have AC energy consumption data in EEI. We calculate country-level f for the 14 countries/regions excluding the U.S.

Among these 14 countries/regions, 11 have total energy consumption data available in WEB. These are: South Korea, Germany, Japan, France, Portugal, New Zealand, Italy, Morocco, Netherlands, Canada, and Spain. For each of these countries/regions, f is calculated as:

$$f = \frac{E_{AC,res} + E_{AC,com}}{E_{tot}}, \quad \text{(S1)}$$

where $E_{AC,res}$ and $E_{AC,com}$ are average annual AC energy consumption for residential and commercial sectors, respectively, and E_{tot} is the average annual total primary energy consumption. The average is computed for 2010 - 2019 ignoring missing years.

For the remaining 3 countries/regions without E_{tot} data, which include Uruguay, Taiwan, and Hong Kong, we approximate total primary energy consumption with total final energy consumption (i.e., energy conversion and transmission losses are excluded), and calculate f as:

$$f = \frac{E_{AC,res} + E_{AC,com}}{E_{res} + E_{com} + E_{ind} + E_{tra}}, \quad \text{(S2)}$$

where E_{res}, E_{com}, E_{ind} and E_{tra} are average annual total energy consumption for residential, commercial, industrial, and transportation sectors, respectively.

U.S. subcountry-level data come from three EIA datasets: 1) 2015 Residential Energy Consumption Survey (RECS) (https://www.eia.gov/consumption/residential/data/2015/), which include the annual final end-use (including AC) energy consumption in the residential sector at the census division level (the 50 U.S. states are grouped into 9 census divisions); 2) 2018 Commercial Buildings Energy Consumption Survey (CBECS) (https://www.eia.gov/consumption/commercial/data/2018/), which include the annual final end-use (including AC) energy consumption in the commercial sector at the census division level, and 3) 2020 State Profiles and Energy Estimates (https://www.eia.gov/state/), which include annual total primary energy consumption for all sectors (including residential, commercial, transportation, and industrial) at the state level.

We combine the three datasets and calculate f for each state as:

$$f = \frac{E'_{AC,res}}{E'_{res}} \cdot \frac{E_{res}}{E_{tot}} + \frac{E'_{AC,com}}{E'_{com}} \cdot \frac{E_{com}}{E_{tot}}, \quad \text{(S3)}$$

where the prime symbol denotes the census-division value of the respective quantity is used. This allows us to obtain state-level estimates of f by leveraging census-division level statistics where state-level information is missing.

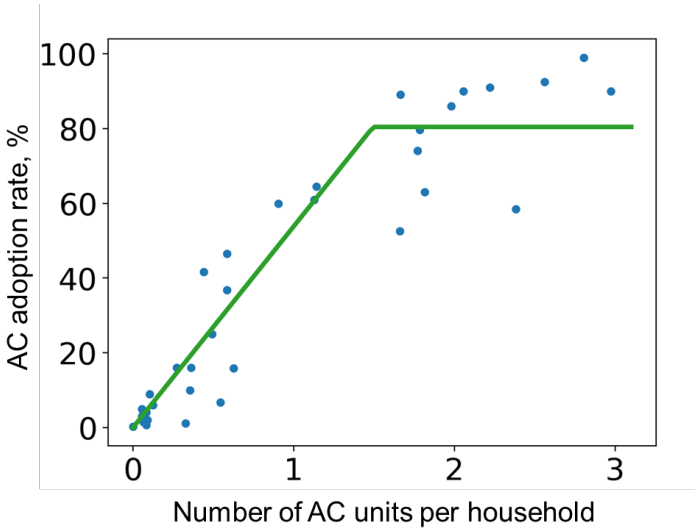

Figure S1. The linear model fit between AC adoption rate and number of AC units per household for 34 countries.

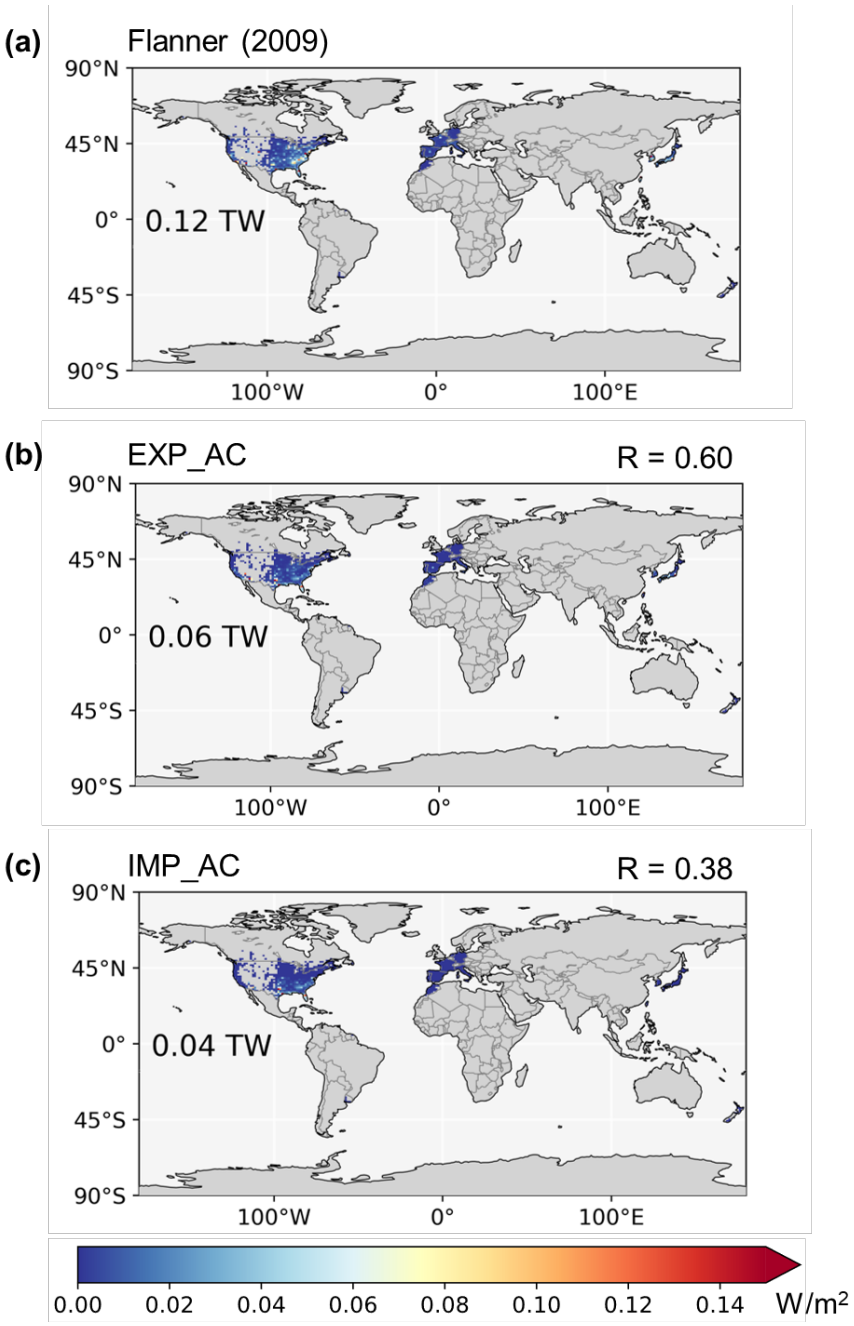

933

934 **Figure S2**. Improvements in modeled anthropogenic heat flux due to AC for available

935 countries/regions in 2010 - 2014. (a), observational estimates derived from Flanner

936 (2009), (b) modeled AHF due to AC using the new explicit-AC-adoption scheme

937 (EXP_AC), and (c) modeled AHF due to AC using the original implicit-AC-adoption

scheme (IMP_AC). Numbers in panels represent the total anthropogenic heat plotted in each panel. R is the pattern correlation between each panel and panel (a).

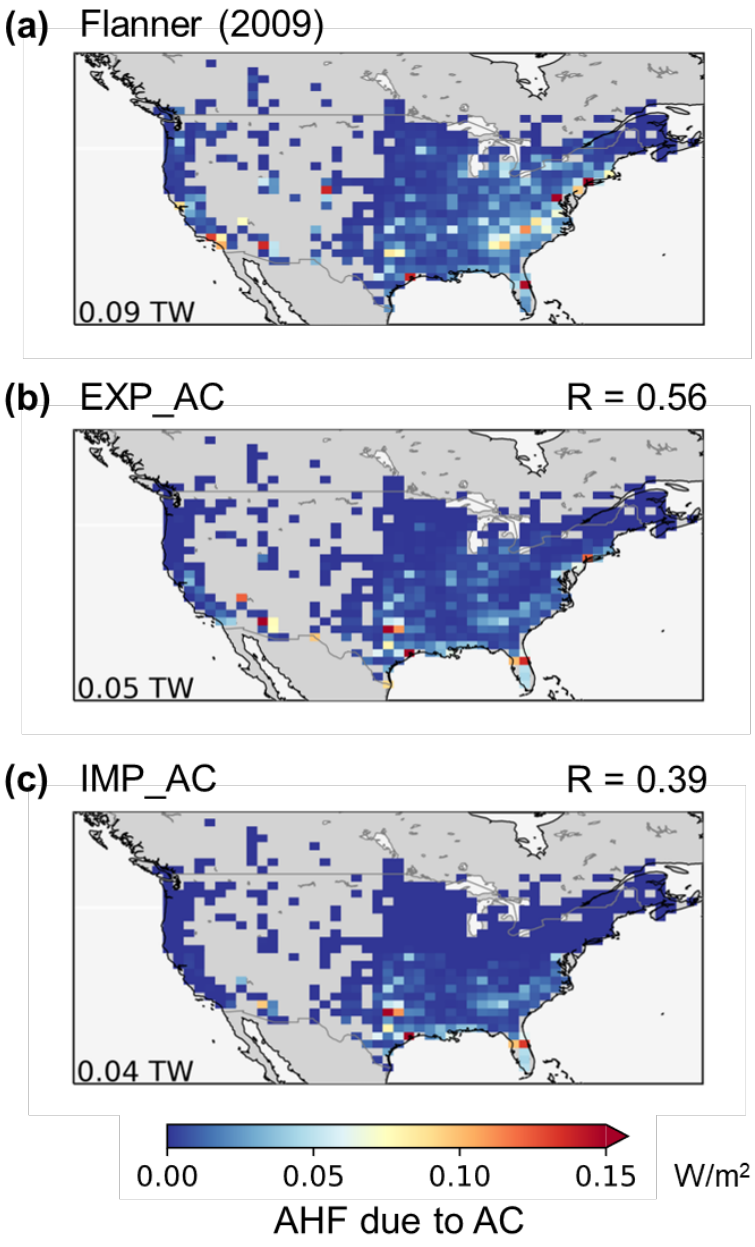

Figure S3. As in Figure S2 but for Contiguous US and parts of Canada.

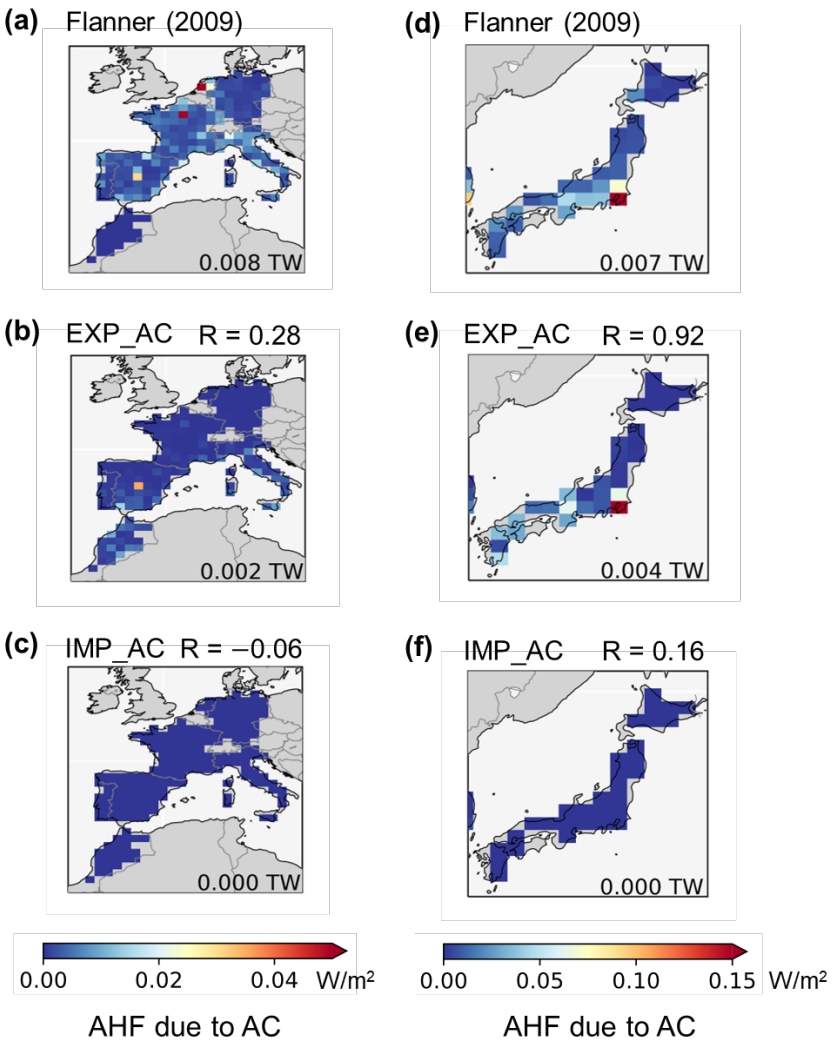

944

945 **Figure S4**. As in Figure S2 but for (a-c) Europe and North Africa, and (d-f) Japan.

946

947 **Table S1**. Air-conditioning (AC) adoption rate data sources.

Country/region	Data year	Data source
AC adoption rate		
Japan	2018	IEA, Percentage of households equipped with AC in selected countries, 2018, IEA, Paris https://www.iea.org/data-and-statistics/charts/percentage-of-households-equiped-with-ac-in-selected-countries-2018, IEA. License: CC BY 4.0
United States *(country level)*		
Korea		
Saudi Arabia		
China *(country level)*		
Mexico		
Brazil		
Indonesia		
South Africa		
India		
Argentina	2010	Davis, L., Gertler, P., Jarvis, S. & Wolfram, C. Air conditioning and global inequality. Global Environmental Change 69, 102299 (2021). https://doi.org/10.1016/j.gloenvcha.2021.102299
El Salvador		
Germany		
Ghana		
Nigeria		
Pakistan		
Paraguay		
Russia		
Sierra Leone		
Uruguay		

Hong Kong	2012	Gao, Y., Chan, E. Y. Y., Lam, H. C. Y., & Wang, A. (2020). Perception of Potential Health Risk of Climate Change and Utilization of Fans and Air Conditioners in a Representative Population of Hong Kong. International Journal of Disaster Risk Science, 11(1), 105–118. https://doi.org/10.1007/s13753-020-00256-z
Canada	2019	Statistics Canada, Environment, Energy and Transportation Statistics Division, Air Conditioners, 2023. https://www150.statcan.gc.ca/t1/tbl1/en/tv.action?pid=3810001901
Australia *(country and state levels)*	2014	Australia Bureau of Statistics, Environmental Issues: Energy Use and Conservation, 2014, Table 5. https://www.abs.gov.au/AUSSTATS/abs@.nsf/DetailsPage/4602.0.55.001Mar%202014?OpenDocument
Israel	2015	Israel Central Bureau of Statistics, Table 14, Ownership of Durable Goods in Deciles of Households by Net Income Per Standard Person, 2015, https://www.cbs.gov.il/he/publications/DocLib/2017/1677/t14.pdf
Singapore	2017/18	Singapore Department of Statistics, Report on the Household Expenditure Survey, 2019, Chart 3.6. https://www.singstat.gov.sg/-/media/files/publications/households/hes201718.ashx
Malta	2010	Malta National Statistics Office, Development of Detailed Statistics on Energy Consumption in Households, Table 4, https://cros-legacy.ec.europa.eu/system/files/SECH_Project_Malta.pdf
Bangladesh	2019	Asia Frontier Capital, AFC Asia Frontier Fund: 2019 Review and Outlook for 2020, 2019. https://www.asiafrontiercapital.com/2019/406-newsletter-issue-103-review-2019-and-outlook-2020.html
Sri Lanka		
Thailand	Between 2010 and 2019	Enerdata, The Future of Air-Conditioning, 2019, Figure 2. https://www.enerdata.net/publications/executive-briefing/the-future-air-conditioning-global-demand.html
Malaysia		
Spain		
Turkey		
Italy		Enerdata and Davis et al. (2021)
Greece	2015	The Seattle Times, Hotter days, but much of Europe still cool toward air conditioning, 2015. https://www.seattletimes.com/nation-world/hotter-days-but-much-of-europe-still-cool-toward-air-conditioning/
Taiwan	2015	National Bureau of Statistics of China, China Statistical Yearbook 2016, Chapter 28. http://www.stats.gov.cn/sj/ndsj/2016/indexeh.htm
United States *(by state)*	2020	U.S. Energy Information Administration, Residential Energy Consumption Survey 2020, Highlights for air conditioning in U.S. homes by state, 2020, https://www.eia.gov/consumption/residential/data/2020/index.php?view=state
Number of AC units per household		

196 Countries	2010 - 2018	IEA, Is cooling the future of heating?, 2020, IEA, Paris https://www.iea.org/commentaries/is-cooling-the-future-of-heating, IEA. License: CC BY 4.0
China *(by province)*	2015	National Bureau of Statistics of China, China Statistical Yearbook 2016, Chapter 6. http://www.stats.gov.cn/sj/ndsj/2016/indexeh.htm

948